Rheol Acta (2003) 42: 326–337
DOI 10.1007/s00397-002-0288-1

ORIGINAL CONTRIBUTION

Brian J. Edwards
Marco Dressler

A rheological model with constant approximate volume for immiscible blends of ellipsoidal droplets

Received: 29 July 2002
Accepted: 13 November 2002
Published online: 1 February 2003

B.J. Edwards (✉)
Department of Chemical Engineering,
The University of Tennessee,
Knoxville, TN37996, USA
E-mail: bjedwards@chem.engr.utk.edu

M. Dressler
Institute of Food Science, ETH-Zürich,
CH-8000, Zürich, Switzerland

Abstract We develop a set of evolution equations describing the effects of a general deformation field on the shape, size, and orientation of constant-volume droplets suspended in a Newtonian fluid. The rheological characteristic functions of this incompressible and immiscible polymer blend model are also derived in tandem with the above-mentioned set. The constant-volume constraint is implemented using a recent methodology (Edwards BJ, Dressler M, Grmela M, Ait-Kadi A (2002) Rheological models with microstructural constraints. Rheo Acta (in press)) and discussed relative to the similarly volume-constrained model of Almusallam et al. (Almusallam AS, Larson RG, Solomon MJ (2000). A constitutive model for the prediction of ellipsoidal droplet shapes and stresses in immiscible blends. J Rheol 44:1055–1083). Sample results are reported for step-strain and shear relaxation profiles.

Keywords Polymer blends · Constant volume models · Rheological characterization · Blend relaxational phenomena

Introduction

The flow properties and microstructural characteristics of immiscible phases is of interest in many fields of science and technology, and especially so with regard to the physical properties of processed polymer blends. Over the past decade, several notable attempts have been made to model the orientational and deformational dynamics of the dispersed phase, and to couple this dynamics with a rheological equation of state for describing the mechanical properties of the deforming microstructure (Doi and Ohta 1991; Wagner et al. 1999; Grmela and Ait-Kadi 1994, 1998; Grmela et al. 1998, 2001; Almusallam et al. 2000; Maffettone and Minale 1998; Lee and Park 1994; Bousmina et al. 2001). These models are typically written for blends composed of equidensity and equiviscosity Newtonian fluids, with a second-rank tensor describing the shape and orientation of the interfacial area between the two fluids. Consequently, two immediately identifiable physical shortcomings are evident. First, the fluids under investigation are not Newtonian, and thus any model behavior predicted at relatively high deformations is circumspect. Second, the volume of the dispersed phase, as quantified by the second-rank tensor variable, is allowed to vary, even though the blended fluids are believed to be incompressible.

To make up for the second shortcoming, Almusallam et al. (2000) have recently derived a model for equidensity Newtonian polymer blends that enforces a constraint upon the time evolution of the second-rank tensor variable. This constraint approximates the volume of the dispersed phase, but is not the true volume. A true constant volume constraint has been implemented in rheological models on occasions in the past (Leonov 1976; Ait-Kadi et al. 1999; Edwards et al. 2002), but has only been incorporated into a specific model for polymer blends on a single occasion (Maffettone and Minale 1998).

Recently, a methodology has been developed (Edwards et al. 2002) that allows for the direct incorporation of microstructural constraints into the derivation of mutually consistent dynamical evolution equations for microstructural variables and the corresponding rheological properties. Presently, this methodology is used for the purpose of deriving a simpler (with regard to ease of use) version of the model of Almusallam et al. (2000), which also appears to shore up some inadequacies of the previous model, as explained below.

Microstructural variables and models for polymer blends

The first theoretical development to have a significant impact on the description of polymer blends was the introduction of the Doi-Ohta (DO) Model (Doi and Ohta 1991). This equidensity, equiviscosity, Newtonian model of incompressible, isothermal, and spatially homogeneous polymer blends was written in terms of a second-rank tensor, $\overline{\mathbf{nn}}$, representing the average dyadic product of the unit normal to the interfacial area separating the two fluids. In terms of this entity, two pertinent variables were defined to quantify the dynamical evolution and resulting stress within the blend:

$$Q \equiv \operatorname{tr} \overline{\mathbf{nn}}, \quad \mathbf{q} \equiv \overline{\mathbf{nn}} - \frac{Q}{3}\delta. \tag{1}$$

As defined by these expressions, the scalar Q quantifies the amount of interfacial area and the second-rank tensor $\mathbf{q}$ describes its orientation and anisotropy.

The dynamical evolution equations for these quantities,

$$\begin{aligned} \frac{\partial Q}{\partial t} &= \left.\frac{\partial Q}{\partial t}\right|_{conv} + \left.\frac{\partial Q}{\partial t}\right|_{relax}, \\ \frac{\partial q_{\alpha\beta}}{\partial t} &= \left.\frac{\partial q_{\alpha\beta}}{\partial t}\right|_{conv} + \left.\frac{\partial q_{\alpha\beta}}{\partial t}\right|_{relax}, \end{aligned} \tag{2}$$

consist of both a convective and relaxational mechanism. The first terms on the right-hand sides of the above expressions describe the convection of the interfacial area and shape, respectively:

$$\begin{aligned} \left.\frac{\partial Q}{\partial t}\right|_{conv} &= -q_{\alpha\beta}\nabla_\alpha v_\beta, \\ \left.\frac{\partial q_{\alpha\beta}}{\partial t}\right|_{conv} &= -q_{\alpha\gamma}\nabla_\beta v_\gamma - q_{\beta\gamma}\nabla_\alpha v_\gamma + \frac{2}{3}\delta_{\alpha\beta}q_{\gamma\varepsilon}\nabla_\gamma v_\varepsilon \\ &\quad - \frac{Q}{3}\left(\nabla_\alpha v_\beta + \nabla_\beta v_\alpha\right) + \frac{1}{Q}q_{\alpha\beta}q_{\gamma\varepsilon}\nabla_\gamma v_\varepsilon. \end{aligned} \tag{3}$$

The second expression is indicative of a tensor that deforms covariantly. The relaxational contributions to the evolution equations are given by

$$\begin{aligned} \left.\frac{\partial Q}{\partial t}\right|_{relax} &= -c_1\frac{\Gamma}{\eta_0}Q^2, \\ \left.\frac{\partial q_{\alpha\beta}}{\partial t}\right|_{relax} &= -(c_1 + c_2)\frac{\Gamma}{\eta_0}Q\, q_{\alpha\beta}, \end{aligned} \tag{4}$$

where Γ is the interfacial surface tension (energy/area), η_0 is the viscosity of both fluids, and c_1, c_2 are phenomenological constants. According to these expressions, the interfacial surface energy strives to decrease the amount of interfacial area, Q, and to drive the system toward the isotropic state.

The relaxation expressions of Eq. (4) are able to describe the demixing effect of continuous blends, but are not appropriate for describing the anisotropic and rheological response of dispersed phases in which one fluid exists as droplets within the other. For this case, another area relaxation term is used that prohibits further changes in the shape of the droplets once they have become spherical:

$$\left.\frac{\partial Q}{\partial t}\right|_{relax} = -\frac{c_1\Gamma}{\eta_0}Q\left(q_{\alpha\beta}q_{\alpha\beta}\right)^{1/2}. \tag{5}$$

In conjunction with, but independently of, the evolution equations described above, an expression for the rheological properties of the blend was derived as well. The extra stress tensor of the DO Model quantifies the effects of the interfacial area and shape upon the blend's rheological characteristic functions:

$$\begin{aligned} \sigma_{\alpha\beta} &= \eta_m\left(\nabla_\alpha v_\beta + \nabla_\beta v_\alpha\right) - \Gamma\, q_{\alpha\beta} \\ &\quad - \frac{\eta_m - \eta_d}{V}\int \left(u_\alpha n_\beta + n_\alpha u_\beta\right) dS. \end{aligned} \tag{6}$$

In this expression, $\mathbf{u}$ is the local fluid velocity at the interface, η_m is the matrix phase viscosity, and η_d is the dispersed phase viscosity. The first term in this expression is the stress contribution arising from the Newtonian fluid. The second and third terms were derived by Batchelor (1970) as the interfacial tension contributions arising due to the hydrodynamic interaction at the droplet surface. For an equiviscosity blend, the third term on the right-hand side of this expression vanishes. Equation (6) was used by Onuki (1987) to describe stresses and viscosities in phase separating fluids near the critical point.

Several attempts to improve upon the DO Model were made over the previous decade, each trying to obtain more realistic relaxation expressions over Eqs. (4) and (5) without changing the microstructural variables Q and $\mathbf{q}$ (Grmela and Ait-Kadi 1998; Grmela et al. 1998; Lacroix et al. 1998; Wagner et al. 1999; Lee and Park 1994). Lee and Park (1994) modified the DO model to incorporate additional relaxation mechanisms to Eq. (4). Grmela and Ait-Kadi (1994) (see errata in Grmela and Ait-Kadi 1998) derived a dynamical evolution equation for a new variable,

$$\mathbf{c} \equiv Q\mathbf{q} + \frac{1}{3}\, Q^2\, \delta, \tag{7}$$

that deforms as a covariant tensor. They argued that, according to Eq. (1), the variables Q and $\mathbf{q}$ are interrelated through the dyad $\overline{\mathbf{nn}}$: note that $\mathrm{tr}\mathbf{c} = Q^2$. By using the Poisson bracket for a covariant deformation tensor, they were able to derive a dynamical evolution equation for this tensor, and its corresponding expression for the extra stress tensor. The evolution equation was of the DO type; however, the extra stress tensor expression had an additional term over the Batchelor expression, Eq. (6). Note, however, that the expressions for the lower-convected derivatives appearing in Grmela and Ait-Kadi (1994, 1998) are incorrect, as are the corresponding Poisson brackets. The correct form of the lower-convected Poisson bracket can be found in Appendix B of Beris and Edwards (1990a) and Appendix C of Beris and Edwards (1994). Lastly, Wagner et al. (1999) retained the independence of the DO variables, yet applied the GENERIC formalism (Grmela and Öttinger 1997; Öttinger and Grmela 1997) to obtain additional relaxation mechanisms allowing for better representations of flow start-up behavior and blends in which the coalescence and break-up of droplets is suppressed.

More recent theoretical work in this area has begun to take into consideration the physically intuitive notion that an incompressible fluid should have a constant volume. In other words, if a second-rank tensor field is used to describe the microstructure of the dispersed phase, then this tensor must be constrained in some fashion so that the volume of the dispersed phase remains constant. Furthermore, recent work has started to consider blends on polymers that are not equiviscosity. Maffettone and Minale (1998) introduced a model with such a constraint, but in terms of a second-rank tensor, $\mathbf{S}$, which is effectively the inverse of the DO tensor $\mathbf{q}$. Thus the mutually perpendicular eigenvalues of $\mathbf{S}$ describe the orientation and shape of the dispersed phase droplets, and the determinant quantifies their volumes. $\mathbf{S}$ is thus a contravariant deformation tensor, although Maffettone and Minale consider a non-affinely convecting microstructure.

In the Maffettone and Minale (MM) Model (Maffettone and Minale 1998), the evolution equation for the microstructural variable is

$$\frac{\partial S_{\alpha\beta}}{\partial t} + v_\gamma \nabla_\gamma S_{\alpha\beta} + W_{\alpha\gamma} S_{\gamma\beta} - S_{\alpha\gamma} W_{\gamma\beta} - f_2\left(D_{\alpha\gamma} S_{\gamma\beta} + S_{\alpha\gamma} D_{\gamma\beta}\right) = -\frac{\mathrm{f}_1}{\tau}\left[S_{\alpha\beta} - \mathrm{g}\, \delta_{\alpha\beta}\right], \tag{8}$$

where $\mathbf{D}$ and $\mathbf{W}$ are the symmetric and antisymmetric contributions to the velocity gradient tensor field, respectively. Also in this expression, $\tau \equiv \eta_\mathrm{m} \mathrm{r}_0/\Gamma$ is a characteristic time constant of the droplet shape relaxation, f_1 is a phenomenological constant that depends on the viscosity ratio of the dispersed and matrix phases, $\mathrm{M} \equiv \eta_\mathrm{d}/\eta_\mathrm{m}$, and $\mathrm{g}(\mathbf{S})$ is a function that guarantees that the volume of the droplets is constant:

$$\mathrm{g} = 3\frac{III_S}{II_S}. \tag{9}$$

In Eq. (9), the numerator is the third invariant of $\mathbf{S}$, i.e., the determinant, and the denominator is the second, $\mathrm{II}_\mathrm{S} = \frac{1}{2}\left[S_{\alpha\alpha}^2 - S_{\alpha\beta}S_{\alpha\beta}\right]$. As mentioned above, the tensor $\mathbf{S}$ is physically a contravariant deformation tensor. However, due to the implementation of the non-affine motion assumption, the usual upper-convected derivative in the evolution equation for $\mathbf{S}$ has been replaced with the modified Jaumann, or corotational, derivative, in terms of the phenomenological parameter f_2. When $\mathrm{f}_2 = 1$ and $\tau \to \infty$, the upper-convected time derivative is recovered. Note that the MM Model does not provide a relationship for the extra stress tensor field. A relationship for the corresponding extra stress tensor was derived by Grmela et al. (2001).

In order to return to DO-type variables, and at the same time provide a compatible expression for the extra stress tensor while maintaining the constant volume constraint, Almusallam et al. (2000) derived a new model for polymer blends. The Almusallam-Larson-Solomon (ALS) Model is written in terms of an anisotropy tensor that is not traceless,

$$\hat{\boldsymbol{q}}_{\alpha\beta} \equiv \frac{1}{V_d}\int n_\alpha n_\beta\, d^2 n, \tag{10}$$

where the average is normalized with respect to the droplet volume, V_d. The surface area is still defined analogously to Eq. (1), $\hat{\mathbf{Q}} \equiv \mathrm{tr}\,\hat{\mathbf{q}}$. With these variables, the Batchelor expression for the extra stress tensor field is modified to

$$\sigma_{\alpha\beta} = \eta_0\left(\nabla_\alpha v_\beta + \nabla_\beta v_\alpha\right) - \phi\,\Gamma\left(\hat{\boldsymbol{q}}_{\alpha\beta} - \frac{1}{3}\,\hat{\boldsymbol{q}}_{\gamma\gamma}\,\delta_{\alpha\beta}\right). \tag{11}$$

where ϕ is the volume fraction of the droplets. The evolution equation for the anisotropy tensor in the affine deformation case is given by

$$\frac{\partial \hat{\boldsymbol{q}}_{\alpha\beta}}{\partial t} = \left.\frac{\partial \hat{\boldsymbol{q}}_{\alpha\beta}}{\partial t}\right|_{conv} + \left.\frac{\partial \hat{\boldsymbol{q}}_{\alpha\beta}}{\partial t}\right|_{relax} \tag{12}$$

where

$$\left.\frac{\partial \hat{\boldsymbol{q}}_{\alpha\beta}}{\partial t}\right|_{conv} = -v_\gamma \nabla_\gamma \hat{\boldsymbol{q}}_{\alpha\beta} - \hat{\boldsymbol{q}}_{\alpha\gamma}\nabla_\beta v_\gamma - \hat{\boldsymbol{q}}_{\beta\gamma}\nabla_\alpha v_\gamma + \frac{1}{\hat{\boldsymbol{q}}_{\varsigma\varsigma}}\hat{\boldsymbol{q}}_{\alpha\beta}\hat{\boldsymbol{q}}_{\gamma\varepsilon}\nabla_\gamma v_\varepsilon, \tag{13}$$

$$\left.\frac{\partial \hat{\boldsymbol{q}}_{\alpha\beta}}{\partial t}\right|_{relax} = -\frac{f(M,\phi)\,\Gamma\,\hat{\boldsymbol{q}}_{\alpha\gamma}^n\left[\hat{\boldsymbol{q}}_{\gamma\beta} - g(\mathbf{q})\,\delta_{\gamma\beta}\right]}{\eta_m\left[III_{\hat{\boldsymbol{q}}}\left(10\, II_{\hat{\boldsymbol{q}}}^{3}/2 + I_{\hat{\boldsymbol{q}}}^3\right)\right]^{(n-1)/6}}. \tag{14}$$

In these expressions, $n = 3/2$, and the Choi-Schowalter expression (Choi and Schowalter 1975) was used to determine the empirical function,

$$f(M,\phi)=\frac{160\,(27+30\sqrt{3})^{(n-1)/6}\,(M+1)^2}{(19M+16)\,(8M^2+5\,(19\,\phi+4)\,M+4\,(20\,\phi+3))}. \tag{15}$$

The function $g(\hat{\mathbf{q}})$ was determined as explained below. The evolution equation for $\hat{Q}$, if desired, can be obtained by taking the trace of Eqs. (12), (13), and (14).

With the anisotropy tensor $\hat{\mathbf{q}}$ defined as in Eq. (10) above, the volume of the droplet is not so easily deduced as in the MM Model. Almusallam et al. (2000) thus *approximate* the volume of the droplet as

$$V_d = \frac{c}{\sqrt{III_{\hat{q}}\left(10\,II_{\hat{q}}^{3/2}+I_{\hat{q}}^3\right)}}, \tag{16}$$

where the constant $c = 4\pi/3\left(27+30\sqrt{3}\right)^{\frac{1}{2}}$. To reiterate, this expression for the volume is only approximate, and only applicable to ellipsoidal droplets. As in the MM Model, the function $g(\hat{\mathbf{q}})$ acts to guarantee that the evolution equation for $\hat{\mathbf{q}}$, Eqs. (12), (13), and (14), belongs to the space where the approximate volume, V_d, is conserved. One realization of this function can be derived by requiring the time derivative of V_d to vanish at all times. This leads to a very long expression for $g(\hat{\mathbf{q}})$:

$$\begin{aligned}
g(\hat{\mathbf{q}}) = {} & (6III_{\hat{q}}\hat{q}_{12}^{3/2}(I_{\hat{q}}^2+5\sqrt{II_{\hat{q}}}\hat{q}_{33})\hat{q}_{12}+III_{\hat{q}}\sqrt{II_{\hat{q}}} \\
& (-30\hat{q}_{12}^2\hat{q}_{11}^{3/2}+15\hat{q}_{12}^{3/2}\hat{q}_{11}\hat{q}_{12}+15\hat{q}_{22}(\hat{q}_{11}^{3/2}+\hat{q}_{22}^{3/2})\hat{q}_{11} \\
& -15\hat{q}_{12}^{3/2}\hat{q}_{22}\hat{q}_{12})+3III_{\hat{q}}\hat{q}_{11}(I_{\hat{q}}^2\hat{q}_{11}^{3/2}+5\sqrt{II_{\hat{q}}}\hat{q}_{33}(\hat{q}_{11}^{3/2} \\
& +q_{33}^{3/2}))+(10II_{\hat{q}}^{3/2}+I_{\hat{q}}^3)(-\hat{q}_{12}^{3/2}\hat{q}_{22}\hat{q}_{33}\hat{q}_{12} \\
& +\hat{q}_{33}(-2\hat{q}_{11}^{3/2}-\hat{q}_{33}^{3/2})\hat{q}_{12}^2+\hat{q}_{11}\hat{q}_{12}^{3/2}\hat{q}_{33}\hat{q}_{12} \\
& +\hat{q}_{11}\hat{q}_{22}\hat{q}_{33}(\hat{q}_{11}^{3/2}+\hat{q}_{22}^{3/2}+\hat{q}_{33}^{3/2}))+3III_{\hat{q}} \\
& \times(I_{\hat{q}}^2\hat{q}_{33}^{3/2}\hat{q}_{33}+\hat{q}_{22}(I_{\hat{q}}^2\hat{q}_{22}^{3/2}+5\sqrt{II_{\hat{q}}}\hat{q}_{33}(\hat{q}_{22}^{3/2}+\hat{q}_{33}^{3/2}))) \\
& \div(3III_{\hat{q}}(\hat{q}_{11}^{3/2}+\hat{q}_{22}^{3/2}+\hat{q}_{33}^{3/2})I_{\hat{q}}^2+(10II_{\hat{q}}^{3/2}+I_{\hat{q}}^3) \\
& \times(\hat{q}_{22}\hat{q}_{33}\hat{q}_{11}^{3/2}+\hat{q}_{22}\hat{q}_{11}\hat{q}_{33}^{3/2}+\hat{q}_{11}\hat{q}_{33}\hat{q}_{22}^{3/2} \\
& -2\hat{q}_{12}^{3/2}\hat{q}_{33}\hat{q}_{12}-\hat{q}_{12}^2\hat{q}_{33}^{3/2})+15III_{\hat{q}}\sqrt{II_{\hat{q}}} \\
& \times(\hat{q}_{22}\hat{q}_{11}^{3/2}+\hat{q}_{33}\hat{q}_{11}^{3/2}+(\hat{q}_{22}^{3/2}+\hat{q}_{33}^{3/2})\hat{q}_{11} \\
& +\hat{q}_{22}\hat{q}_{33}^{3/2}-2\hat{q}_{12}^{3/2}\hat{q}_{12}+\hat{q}_{22}^{3/2}\hat{q}_{33})).
\end{aligned} \tag{17}$$

Note that this expression, and hence the entire evolution equation for $\hat{\mathbf{q}}$, is limited to situations where the components $\hat{q}_{13} = \hat{q}_{31} = \hat{q}_{23} = \hat{q}_{32} = 0$. Furthermore, note that the constant-volume constraint is applied only to the relaxational part of the evolution equation for $\hat{\mathbf{q}}$, Eq. (14).

As was the case with the original DO Model, the ALS Model rests upon a derivation in which the extra stress tensor and the evolution equation for $\hat{\mathbf{q}}$ were derived independently. Furthermore, the expression for $g(\hat{\mathbf{q}})$ is just one possibility among many, and it is not necessarily the best or simplest of these.

A volume-constrained blend model

The methodology used herein takes advantage of the underlying mathematical structure of a complex fluid that is present on any level of description. This structure has been investigated extensively over the past fifteen years (Grmela and Carreau 1987; Grmela 1988, 1989; Beris and Edwards 1990a, 1990b,1994; Edwards and Beris 1991a, 1991b; Grmela and Öttinger 1997; Öttinger and Grmela 1997; Dressler et al. 1999). Most of this work was concerned with complex fluids that were free of microstructural constraints. Recently, Edwards et al. (2002) extended this methodology to constrained microstructures, and it is natural to apply it to the volume constraint studied by Almusallam et al. (2000). (A detailed description of the methodology may be found in the previous article, so we offer only a limited discussion here.)

For an unconstrained complex fluid, a proper dynamical description can be written in terms of the variable set $\mathbf{f} = (\mathbf{u}, \rho, \mathbf{C})$, where $\mathbf{u}$ is the fluid momentum density ($\mathbf{u} = \rho\mathbf{v}$), ρ the mass density, and $\mathbf{C}$ the "conformation density" ($\mathbf{C} = \rho\mathbf{c}$). The dynamics of an arbitrary functional of these variables, $F = [\mathbf{u}, \rho, \mathbf{C}]$, can then be expressed as

$$\frac{dF}{dt} = \{F,H\} + [F,H], \tag{18}$$

where the Poisson bracket is

$$\begin{aligned}
\{F,H\} = {} & -\int\left[\frac{\delta F}{\delta u_\gamma}\nabla_\beta\left(\frac{\delta H}{\delta u_\beta}u_\gamma\right)-\frac{\delta H}{\delta u_\gamma}\nabla_\beta\left(\frac{\delta F}{\delta u_\beta}u_\gamma\right)\right]d^3r \\
& -\int\left[\frac{\delta F}{\delta \rho}\nabla_\beta\left(\frac{\delta H}{\delta u_\beta}\rho\right)-\frac{\delta H}{\delta \rho}\nabla_\beta\left(\frac{\delta F}{\delta u_\beta}\rho\right)\right]d^3r \\
& -\int\left[\frac{\delta F}{\delta C_{\alpha\beta}}\nabla_\gamma\left(\frac{\delta H}{\delta u_\gamma}C_{\alpha\beta}\right)-\frac{\delta H}{\delta C_{\alpha\beta}}\nabla_\gamma\left(\frac{\delta F}{\delta u_\gamma}C_{\alpha\beta}\right)\right]d^3r \\
& +\int C_{\alpha\gamma}\left[\frac{\delta H}{\delta C_{\alpha\beta}}\nabla_\beta\left(\frac{\delta F}{\delta u_\gamma}\right)-\frac{\delta F}{\delta C_{\alpha\beta}}\nabla_\beta\left(\frac{\delta H}{\delta u_\gamma}\right)\right]d^3r \\
& +\int C_{\beta\gamma}\left[\frac{\delta H}{\delta C_{\alpha\beta}}\nabla_\alpha\left(\frac{\delta F}{\delta u_\gamma}\right)-\frac{\delta F}{\delta C_{\alpha\beta}}\nabla_\alpha\left(\frac{\delta H}{\delta u_\gamma}\right)\right]d^3r,
\end{aligned} \tag{19}$$

and the dissipation bracket is

$$[F,H] = -\int \Lambda_{\alpha\beta\gamma\varepsilon}\frac{\delta F}{\delta C_{\alpha\beta}}\frac{\delta H}{\delta C_{\gamma\varepsilon}}d^3r - \int Q_{\alpha\beta\gamma\varepsilon}\left(\nabla_\alpha\frac{\delta F}{\delta u_\beta}\right)\left(\nabla_\gamma\frac{\delta H}{\delta u_\varepsilon}\right)d^3r - \int L_{\alpha\beta\gamma\varepsilon}\left[\left(\nabla_\alpha\frac{\delta F}{\delta u_\beta}\right)\frac{\delta H}{\delta C_{\gamma\varepsilon}} - \left(\nabla_\alpha\frac{\delta H}{\delta u_\beta}\right)\frac{\delta F}{\delta C_{\gamma\varepsilon}}\right]d^3r. \tag{20}$$

The Poisson bracket of Eq. (19) is different than in Edwards et al. (2002) in that the current version is for a covariant deformation tensor (Beris and Edwards 1990a, 1994). The quantities Λ and $\mathbf{Q}$ appearing in the dissipation bracket are phenomenological matrix operators that quantify the microstructural relaxational effects and viscous dissipation, respectively (Grmela 1988; Beris and Edwards 1990a, 1990b, 1994).

The matrix $\mathbf{L}$ appearing in Eq. (20) approximates the effects of non-affine motion between the droplets and the surrounding fluid. In reality, the presence of non-affine motion is an indication that the variable set used to describe the problem is inadequate. In these cases, the time derivative of the microstructural tensor should be included in the set of dynamical variables (Edwards et al. 1991). It is only when this variable is neglected, and its evolution equation set to zero and solved for $\partial\mathbf{q}/\partial t$, that non-affine motion appears in the reduced variable description. In this paper, we set $\mathbf{L}=\mathbf{0}$ solely to study the basic elements of the proposed model without the added complications of non-affine motion.

To apply this methodology to the volume constraint associated with the constancy of Eq. (16), we first need to find a mapping of the covariant, unconstrained microstructural tensor $\mathbf{C}$ to a variable whose invariants are forced to maintain the proper relationship at all times. Let us multiply the left-hand side of Eq. (16) by a constant such that the initial (quiescent) volume of the microstructure is scaled to unity:

$$V_d = \frac{a}{\sqrt{III_C\left(10\,II_C^{3/2} + I_C^3\right)}} = 1. \tag{21}$$

To ensure that the volume as given by Eq. (21) is unity under all conditions, one can use the mapping

$$\mathbf{C} \rightarrow \mathbf{q} = a^{1/3}\left[III_C\left(10\,II_C^{3/2} + I_C^3\right)\right]^{-1/6}\mathbf{C}. \tag{22}$$

Under this mapping, it is apparent that $a^2 = III_q\left(10II_q^{3/2} + I_q^3\right)$ under all conditions. Accordingly, it is guaranteed that

$$\frac{\partial V_d}{\partial t} = \left[\left(10\,II_q^{3/2} + I_q^3\right)q_{\alpha\beta}^{-1} + 15\,II_q^{1/2}\left(I_q\delta_{\alpha\beta} - q_{\alpha\beta}\right) + 3\,I_q^2\delta_{\alpha\beta}\right]\frac{\partial q_{\alpha\beta}}{\partial t} = 0, \tag{23}$$

provided that the evolution equation for $\partial\mathbf{q}/\partial t$ is derived appropriately. This is very hard to do using traditional methodologies, but quite tractable under the present auspice.

To accomplish the abovementioned derivation of the evolution equation for $\mathbf{q}$, it is necessary to derive the proper functional derivatives appearing in Eqs. (19) and (20) (Edwards et al. 2002). For the mapping of Eq. (22), these functional derivatives are calculated as

$$\frac{\delta F}{\delta C_{\alpha\beta}} \rightarrow a^{1/3}\left[III_C\left(10II_C^{3/2} + I_C^3\right)\right]^{-1/6}\left[\frac{\delta F}{\delta q_{\alpha\beta}} - \frac{1}{6}\frac{\delta F}{\delta q_{\gamma\varepsilon}}q_{\gamma\varepsilon}q_{\alpha\beta}^{-1} - \frac{1}{6a^2}\frac{\delta F}{\delta q_{\gamma\varepsilon}}q_{\gamma\varepsilon}III_q\left\{15\,II_q^{1/2}\left(I_q\delta_{\alpha\beta} - q_{\alpha\beta}\right) + 3\,I_q^2\delta_{\alpha\beta}\right\}\right]. \tag{24}$$

With these definitions, the evolution equations for the variable set $\mathbf{f} = (\rho, \mathbf{u}, \mathbf{q})$ can be obtained as in Edwards et al. (2002):

$$\frac{\partial\rho}{\partial t} = -\nabla_\gamma(\rho v_\gamma), \tag{25}$$

$$\rho\frac{\partial v_\alpha}{\partial t} = -\rho v_\beta\nabla_\beta v_\alpha - \nabla_\alpha p + \nabla_\beta\sigma_{\alpha\beta}, \tag{26}$$

and the evolution equation for $\mathbf{q}$ is given by Eq. (2) with

$$\left.\frac{\partial q_{\alpha\beta}}{\partial t}\right|_{conv} = -v_\gamma\nabla_\gamma q_{\alpha\beta} - q_{\gamma\alpha}\nabla_\beta v_\gamma - q_{\gamma\beta}\nabla_\alpha v_\gamma + \frac{1}{3}q_{\alpha\beta}\nabla_\gamma v_\gamma + \frac{1}{3a^2}q_{\alpha\beta}q_{\gamma\varepsilon}\,III_q\left\{15\,II_q^{1/2}\left(I_q\delta_{\varepsilon\eta} - q_{\varepsilon\eta}\right) + 3\,I_q^2\delta_{\varepsilon\eta}\right\}\nabla_\eta v_\gamma, \tag{27}$$

$$\left.\frac{\partial q_{\alpha\beta}}{\partial t}\right|_{relax} = -\Lambda_{\alpha\beta\gamma\varepsilon}\frac{\delta A}{\delta q_{\gamma\varepsilon}} + \frac{1}{6}\Lambda_{\gamma\varepsilon\eta\rho}q_{\alpha\beta}q_{\gamma\varepsilon}^{-1}\frac{\delta A}{\delta q_{\eta\rho}} + \frac{1}{6a^2}q_{\alpha\beta}\Lambda_{\gamma\varepsilon\eta\rho}\,III_q\left\{15\,II_q^{1/2}\left(I_q\delta_{\gamma\varepsilon} - q_{\gamma\varepsilon}\right) + 3\,I_q^2\delta_{\gamma\varepsilon}\right\}\frac{\delta A}{\delta q_{\eta\rho}}. \tag{28}$$

Equation (27) was obtained from a non-canonical Poisson bracket; it describes the affine advection and deformation of the microstructural variable defined by Eq. (10), as subjected to the constraint of Eq. (16). Ergo, there is no approximation whatsoever appearing in the time evolution equation, Eq. (27). In other words, once the microstructural variable and its corresponding constraint have been determined, the affine spatio-temporal evolution of this variable, in conjunction with

the evolution of the other system variables, is entirely determined by the Poisson bracket. One does not need to apply any closure approximations to the affine deformation. The additional terms appearing in Eq. (27) beyond those normally present for affine deformation appear due to the volume constraint and are thus part of the affine motion for this constrained variable.

The extra stress tensor field appearing in Eq. (26) is defined as

$$\sigma_{\alpha\beta} = Q_{\beta\alpha\gamma\varepsilon}\nabla_\gamma v_\varepsilon - 2q_{\alpha\gamma}\frac{\delta A}{\delta q_{\beta\gamma}} + \frac{1}{3}\delta_{\alpha\beta}q_{\gamma\varepsilon}\frac{\delta A}{\delta q_{\gamma\varepsilon}} + \frac{1}{3a^2}q_{\gamma\alpha}q_{\rho\eta}\, III_q \left\{15\, II_q^{1/2}\left(I_q\delta_{\gamma\beta} - q_{\gamma\beta}\right) + 3\, I_q^2\delta_{\gamma\beta}\right\}\frac{\delta A}{\delta q_{\rho\eta}}, \tag{29}$$

and the pressure according to the standard equilibrium thermodynamical relationship, $p = -a + \rho\frac{\partial a}{\partial \rho}$. In these expressions, the Hamiltonian is assumed to have the form

$$H[\rho, \mathbf{u}, \mathbf{q}] = \int \frac{1}{2\rho}\, u_\gamma u_\gamma\, d^3r + A\,[\rho, \mathbf{q}] = \int \frac{1}{2\rho}\, u_\gamma u_\gamma\, d^3r + \int a(\rho, \mathbf{q})\, d^3r. \tag{30}$$

Once $A[\rho, \mathbf{q}]$ and the operator matrices are specified, the entire set of evolution equations for the polymer blend with the volume-preserving microstructural constraint is completed. Note that the functional derivatives appearing in Eqs. (28) and (29) usually take on the simple form

$$\frac{\delta A}{\delta q_{\alpha\beta}} = \frac{\partial a}{\partial q_{\alpha\beta}}, \tag{31}$$

although sometimes more complicated expressions are required (Beris and Edwards 1994).

Note that the expression for the extra stress tensor, Eq. (29), has an additional term over the expression of the ALS model, Eq. (11). This discrepancy occurs because in a traditional modeling methodology, such as employed by Almusallam et al. 2000), the stress tensor and dynamical evolution equations are derived independently. Thus the microstructural constraint, in this case volume preservation, is not applied directly to the stress tensor field. In the present methodology, both the stress tensor and evolution equations are derived simultaneously using the same underlying mathematical structure imbedded in the Poisson and dissipation brackets. Also note that both the relaxational and convective contributions to the evolution equation for $\mathbf{q}$ satisfy the constraint of Eq. (23), whereas the convective contribution of the ALS model does not do so. Hence the model described above always satisfies the mathematical constraint that Eq. (16) remains constant rigorously, whereas the ALS model does not do so, in general, as illustrated in the next section. However, one should keep in mind that the volume expression used for the constraint, Eq. (16), is only approximately correct and only applicable to ellipsoidal droplets. Thus this approximation is propagated into the current model as well as the ALS Model.

Some comments are also in order about the expression for the extra stress tensor, Eq. (29), and its relationship with the same quantity in the ALS Model and the Batchelor expression, Eq. (6). The first term in Eq. (29) is the viscous contribution to the extra stress tensor. Once $\mathbf{Q}$ has been specified as the isotropic, incompressible dissipation matrix of Eq. (33), below, all three expressions agree. The second, third, and fourth terms on the right-hand side of Eq. (29) are due to the interfacial energy, but for a fluid that is described by a microstructural variable that is constrained to keep Eq. (16) constant. The Batchelor expression was not derived under such a constraint, so the third and fourth terms on the right-hand side of Eq. (29) go beyond the Batchelor expression. These additional terms are also different than the additional term that appears in the ALS Model stress tensor of Eq. (11). It is believed that this discrepancy occurs because the stress tensor of the ALS Model was not derived simultaneously with the evolution equation for the microstructural variable using a properly consistent method, such as embodied by the Poisson bracket.

To continue, we must declare A, $\mathbf{Q}$, and Λ. Although these are arbitrary in the general form of the model above, we choose them here so that the present model matches the ALS Model as closely as possible. Under this directive, we set

$$A = \int \frac{\phi}{2}\, \Gamma\, I_q\, d^3r, \tag{32}$$

$$Q_{\alpha\beta\gamma\varepsilon} = \eta_m\left(\delta_{\alpha\gamma}\delta_{\beta\varepsilon} + \delta_{\alpha\varepsilon}\delta_{\beta\gamma}\right), \tag{33}$$

$$\Lambda_{\alpha\beta\gamma\varepsilon} = \frac{f(M,\phi)}{\eta_m\, \phi\, a^{(n-1)/3}}\left(q^n_{\alpha\gamma}q_{\beta\varepsilon} + q^n_{\alpha\varepsilon}q_{\beta\gamma} + q^n_{\beta\gamma}q_{\alpha\varepsilon} + q^n_{\beta\varepsilon}q_{\alpha\gamma}\right). \tag{34}$$

With these declarations, the extra stress tensor field becomes

$$\sigma_{\alpha\beta} = \eta_m\left(\nabla_\alpha v_\beta + \nabla_\beta v_\alpha\right) - \phi\,\Gamma\, q_{\alpha\beta} + \frac{\phi}{6}\,\Gamma\, I_q\delta_{\alpha\beta} + \frac{5\,\phi}{2\,a^2}\,\Gamma\, I_q^2\, II_q^{1/2}\, III_q\, q_{\alpha\beta} - \frac{5\,\phi}{2\,a^2}\,\Gamma\, I_q\, II_q^{1/2}\, III_q\, q_{\gamma\alpha}q_{\gamma\beta} + \frac{\phi}{2\,a^2}\,\Gamma\, I_q^3\, III_q\, q_{\alpha\beta}, \tag{35}$$

and the relaxational contribution to the evolution equation for **q** is

$$\left.\frac{\partial q_{\alpha\beta}}{\partial t}\right|_{relax} = -\frac{\Gamma\, f(M,\phi)}{\eta_m\, a^{(n-1)/3}}\left(q^n_{\alpha\gamma}q_{\beta\gamma} + q^n_{\beta\gamma}q_{\alpha\gamma}\right) + \frac{\Gamma\, f(M,\phi)}{3\,\eta_m\, a^{(n-1)/3}}\, I^n_q\, q_{\alpha\beta} + \frac{\Gamma\, f(M,\phi)}{3\,\eta_m\, a^2\, a^{(n-1)/3}}\, q_{\alpha\beta}\, III_q \times \left(15\, I_q\, II_q^{1/2}\, q^n_{\gamma\varepsilon}q_{\gamma\varepsilon} - 15\, II_q^{1/2}\, q^n_{\gamma\rho}q_{\varepsilon\rho}q_{\gamma\varepsilon} + 3\, I_q^2\, q^n_{\gamma\varepsilon}q_{\gamma\varepsilon}\right). \quad (36)$$

The extra terms appearing in Eq. (36) as compared to the ALS relaxational equation, Eq. (14), are the present model's equivalents of the ALS g function. Note that our relaxation expression, as opposed to the ALS expression, is completely general for arbitrary **q**, i.e., when this tensor possesses a full compliment of components.

Sample calculations

In this section, we wish to explore some of the initial implications of the present model. In order to understand the basic physics of the model, we reduce it to its bare minimum of features. This allows us to grasp more easily the root behavior of the model without having to sort through extraneous issues associated with slight modifications to the core model behavior. To this end, we set the parameter n equal to unity, and $\eta_m = 0$ so that only the elastic contribution to the extra stress tensor is present. Also, we define a modified capillary number as $Ca \equiv \frac{\eta_m r_0}{\Gamma f(M,\phi)\tau}$, so that the function $f(M,\phi)$ is normalized out of the evolution equation for **q**. Also, we effectively remove some of the parameters from the problem by working in terms of dimensionless variables, defined with tildes as $\tilde{q}_{\alpha\beta} = r_0 q_{\alpha\beta}$, $\tilde{t} = t/\tau$, and $\tilde{\nabla}_\alpha \tilde{v}_\beta = \tau \nabla_\alpha v_\beta$.

The resulting dimensionless equations were solved for transient shear flow using a fourth-order Runge-Kutta algorithm. Both start-up and relaxation behavior was examined for various capillary numbers and dimensionless shear rates. In the following paragraphs, we will not place the tildes on all displayed symbols, it being understood that all quantities described are dimensionless.

Figures 1 and 2 show the start up behavior of the anisotropy tensor as a function of shear strain, γ, for one dimensionless shear rate, $\dot{\gamma} = 10$, and three values of the capillary number, $Ca = (1, 10, 100)$. For $Ca = 1$, the steady state of all components is attained after the application of about 15 strain units. For larger capillary numbers, the components do not approach steady-state values until very large shear strains are attained, $\gamma = 120$

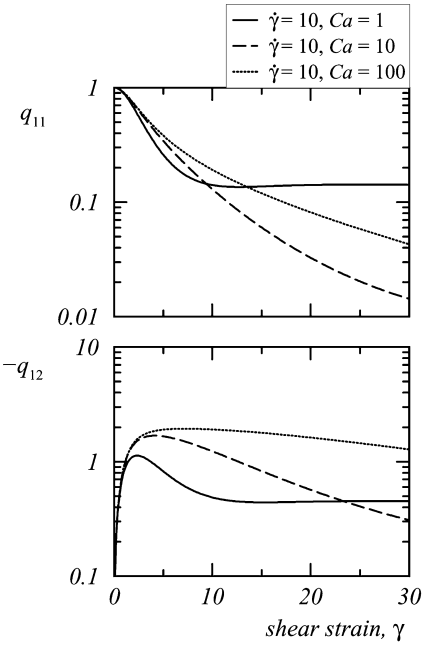

Fig. 1 Dimensionless anisotropy tensor components q_{11} and q_{12} as functions of shear strain for $\dot{\gamma} = 10$ and several capillary numbers after start up of shear flow

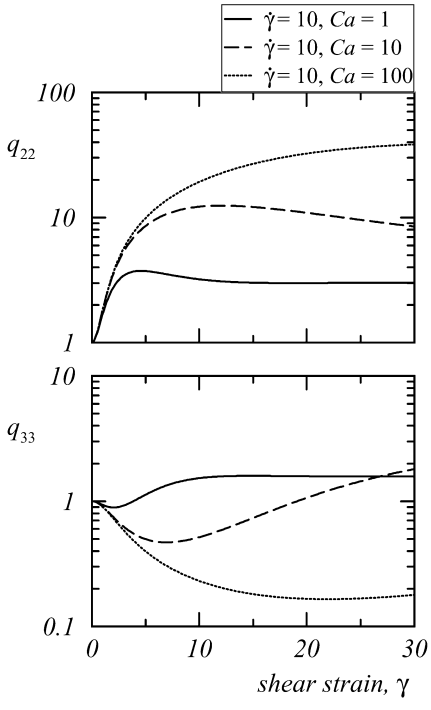

Fig. 2 Dimensionless anisotropy tensor components q_{22} and q_{33} as functions of shear strain for $\dot{\gamma} = 10$ and several capillary numbers after start up of shear flow

for $Ca = 10$ and $\gamma = 300$ for $Ca = 100$. Even at these large strain values, on a logarithmic scale, one can still notice significant variations in the components with time. These large strain values induce such dramatic morphology changes in the droplets that they essentially become very thin sheets. Such changes are probably not realistic physically, but since the model does not allow droplet break up, the mathematical model is forced into an aphysical behavior. Although it appears that the values of some of the components vary in a peculiar non-monotonic way with capillary number, this is not the case. Were the figure abscissas extended to much higher strains, the expected behavior would be observed. This behavior is very similar to that of the ALS Model (Almusallam et al. 2000, Figs. 7 and 8). Since we have set the parameter n equal to unity, rather than the value of 1.5 used by Almusallam et al. (2000), and since we have normalized out the function $f(M, \phi)$, we believe that this qualitative behavior of the **q** components with strain and capillary number is a generic feature of these volume-constrained models. Note that for the ALS Model the qualitative behavior of the diagonal components of **q** seems to be independent of the closure approximation which is employed in the solution of the time evolution equation of the anisotropy tensor. Therefore, it appears evident that this qualitative behavior is also independent of a reasonable choice for a closure approximation. This might be important, as it appears that for higher capillary numbers the ALS Model encounters difficulties in describing the dependency of q_{33}, regardless of the particular closure approximation employed.

Before discussing the viscometric functions obtained with the model, we offer a few remarks on the detailed experiments performed by Almusallam et al. (2000). These authors performed start-up of shearing flow and step-strain relaxation experiments on single polybutadiene (PBd) droplets (with a diameter of 190 microns) in a polydimethylsiloxane (PDMS) matrix at room temperature. It turned out that the morphological properties of polymer blends consisting of a continuous phase and a dispersed droplet phase could be characterized effectively by the average droplet properties that are condensed in the anisotropy tensor. However, as already mentioned, the ALS Model encounters significant difficulties in predicting accurately droplet morphologies in start up of shear flow for high capillary numbers. The rheological properties of droplet morphologies were measured by Almusallam et al. (2000) for concentrated PBd/PDMS blends, which is an effective ensemble of many (ideally) non-interacting droplets. Even for small capillary numbers, the concentrated blends displayed a very complex rheological behavior. At both low and high capillary numbers, the transient shear stress, σ_{12}, approaches steady state very slowly. This type of asymptotic behavior is not described well by the ALS Model, which predicts a rather fast approach to a steady-state value. Furthermore, an experimentally observed overshoot in the shear stress increased strongly with capillary number, which is also not described well by the ALS Model.

The first normal stress difference, N_1, increases non-monotonically showing a steep increase at low shear strains, a weaker increase at high shear strains, and an overshoot in between these two regimes (Almusallam et al. 2000, Fig. 10). This quantity does not reach a steady state in the range of shear strains investigated experimentally. Thus, N_1, could not be predicted with reliability using the ALS Model. Still, older rheological models for polymer blends do not even capture qualitatively the stresses in concentrated PBd/PDMS blends. Therefore, the ALS Model represents a remarkable step towards a more reliable prediction of the blend's viscometric functions. However, more work needs to be done since the ALS Model fails in predicting the stresses quantitatively, even at low capillary numbers. A possible reason for the poor performance of the ALS Model in start up of shear flow is that the convective contribution to the total evolution equation for **q**, Eq. (13), has not been modeled appropriately; i.e., this contribution does not preserve the approximate expression for the volume of the droplets, Eq. (16). This is demonstrated in Fig. 6, below, and also from applying the constraint (Eq. 23) to Eq. (13). In a regime where relaxational contributions to Eq. (12) are negligible with respect to the convective contributions, such as at low strains, the ALS Model will break down in the sense that it will not necessarily fulfill the constant-volume constraint.

Figure 3 shows the shear stress as calculated from Eq. (35) for $\dot{\gamma} = 10$ and three different capillary numbers,

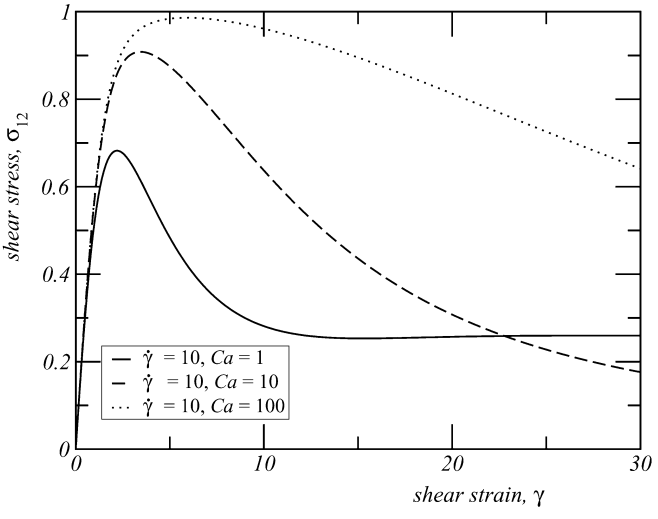

Fig. 3 The elastic shear stress after start-up of shear flow as a function of shear strain for $\dot{\gamma} = 10$ and three different capillary numbers

$Ca = (1, 10, 100)$. The shear stress displays an overshoot, which increases and broadens with increasing capillary number. Notice from Fig. 3 that for higher capillary numbers higher strains have to be applied to reach a steady-state value of the shear stress. Furthermore, our calculations show a rather fast relaxation of the shear stress for low capillary numbers and a slow relaxation for higher capillary numbers. The behavior of the shear stress as a function of shear strain and capillary number is in qualitative agreement with the experiments on concentrated PBd/PDMS blends, and it is similar to the predictions of the ALS Model (Almusallam et al. 2000, Fig. 10). This is evident even though the function $f(M, \phi)$ has been normalized out of our evolution equation.

Figure 4 shows the first and the second normal stress differences for $\dot{\gamma} = 10$ and three different capillary numbers. For the smallest value of the capillary number, the first normal stress difference shows an overshoot at a strain of about 5 and a steady-state value for high shear strains. For the intermediate capillary number, $Ca = 10$, the overshoot shifts towards higher shear strains and the steady-state value is approached rather slowly. For high capillary numbers, the overshoot still appears, shifted to even higher strains, and the steady-state value is reached for even higher shear strains. Note that the first normal stress difference predicted by Eq. (35) is larger in magnitude than the shear stress. This is corroborated by experimental observations on PBd/PDMS blends (Almusallam et al. 2000). The ALS Model makes similar predictions for the relative magnitudes of the shear stress and the first normal stress difference.

The second normal stress difference in Fig. 4 shows a non-linear behavior which is very similar to that of the first normal stress difference. Even the absolute value of this quantity is very similar to that of N_1; however, neither experimental data nor theoretical estimates for N_2 are presented by Almusallam et al. (2000).

In Fig. 5, a comparison is made between the dimensionless shear stress and first normal stress difference for the new model and the ALS Model at a dimensionless shear rate of unity and a low value of the capillary number, $Ca = 1$. According to Jansseune et al. (2001), the ALS Model cannot describe the experimental behavior of their polymer blends in start-up of shear flow at low capillary numbers because it does not attain a steady state at experimentally accessible times—see their Fig. 2 and comments immediately following. As indicated in Fig. 5, the new model seems to alleviate some, if not all, of this deficiency, since it attains a definite steady state, and much more quickly than the ALS Model. The ALS model only approaches a steady state at much high values of strain.

Note that the ALS model presented in this Fig. 5 and the subsequent figure is evaluated in the same simple state as the present model; i.e., $n = 1$, viscous contributions have been neglected, and f has been incorporated into the capillary number. Hence the comparison is meaningful, but limited to the elastic contributions to the extra stress tensor. (Consideration of the viscous

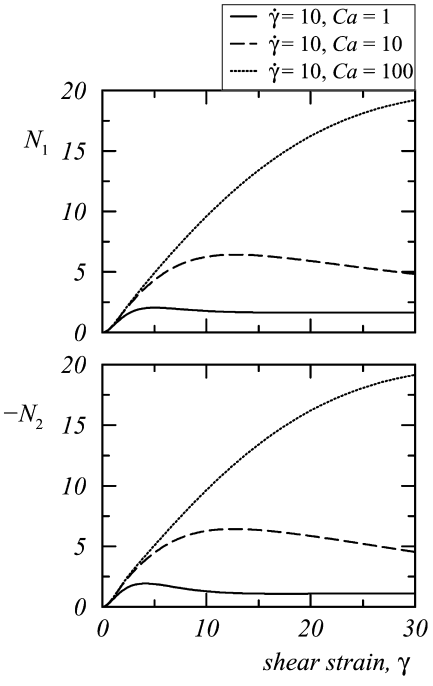

Fig. 4 The normal stress differences after start-up of shear flow as functions of shear strain for $\dot{\gamma} = 10$ and three different capillary numbers

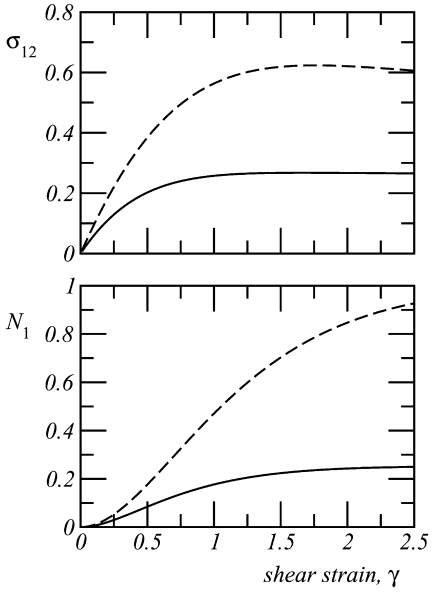

Fig. 5 The dimensionless shear stress and first normal stress difference vs dimensionless shear strain for start-up of shear flow at $\dot{\gamma} = 1$ and $Ca = 1$. The *dashed lines* are the ALS Model predictions and the *solid lines* correspond to the present model

contributions will not change the conclusions anyway.) Thus it appears that the proper specification of the volume conserving constraint in the convective part of the evolution equation is essential for describing the physics of the blends.

In Fig. 6, V_d is plotted vs strain for a dimensionless shear rate of unity and $Ca \to \infty$ for both the ALS Model, Eq. (16), and the current model, Eq. (21). Note that the volume of the ALS Model has been scaled to unity as the strain goes to zero by dividing by $4\pi/3$. When $Ca \to \infty$, the relaxation terms become negligible relative to the convective terms, and only the convective parts of the evolution equations for the microstructural tensors are relevant. As evident in the figure, the current model has a constant value of V_d, whereas the ALS Model does not.

In the remaining figures, we present the relaxational behavior of the models. The ALS Model seems to perform better in relaxation than in start-up of shear flow. The reason for this might be due to the problem mentioned earlier: the convective part of the evolution equation is not volume constrained. In relaxation experiments, the convective contribution to the evolution equation is negligible relative to the relaxational contribution.

Figure 7 shows the relaxation of the diagonal components of the anisotropy tensor for $Ca = 10$ after a step shear of $\gamma = 15$ with two different shear rates, $\dot{\gamma} = (1, 10)$. Similarly to the ALS Model, the thermodynamically consistent model qualitatively describes the anisotropy data for relaxation without the $f(M, \phi)$ function or a non-unit value of n. Note that the model also predicts qualitatively the complicated relaxational behavior of the constant-volume droplets as observed in the experiments. The lengths of the smaller two droplet axes (corresponding to the two largest diagonal components of **q**), relax to equivalent values before the relaxation of all three axes to the isotropic state occurs: there is an initial fast relaxation followed by a second, slower relaxation process. The first arrow in Fig. 7 marks the position where the initial relaxation process is completed and the droplet has recovered an axisymmetric shape. The second arrow marks the point where the droplet has resumed a spherical shape. The description of this two-stage relaxation process is a stringent test for any constrained-volume model, as pointed out by Almusallam et al. (2000). It is satisfied also by the MM Model, but not by the DO Model which does not satisfy volume preservation.

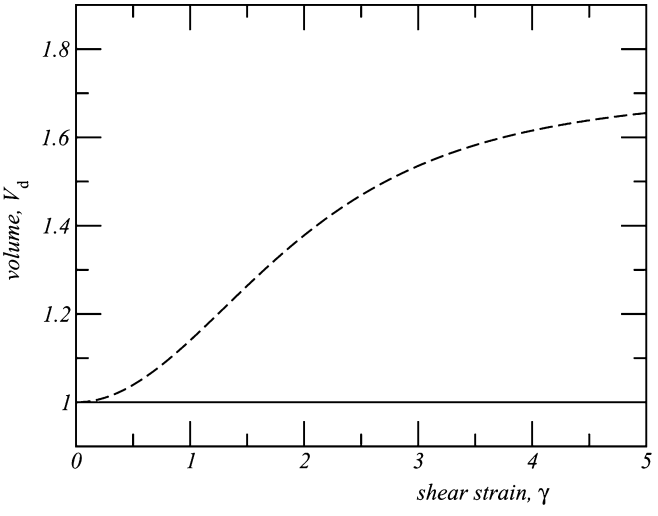

Fig. 6 The droplet volume plotted vs dimensionless strain for $\dot{\gamma} = 1$ and $Ca \to \infty$. The *dashed line* is the ALS Model volume and the *solid line* is the present model volume

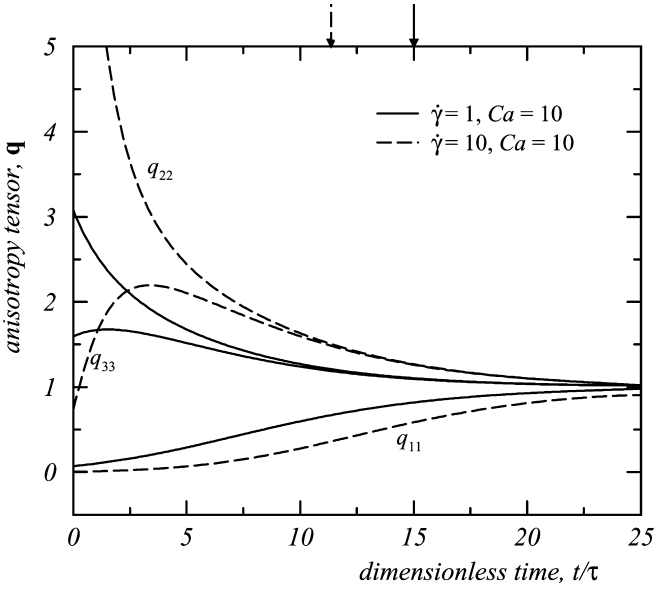

Fig. 7 The diagonal components of the anisotropy tensor as functions of time after a step strain of $\gamma = 15$ for two different shear rates and $Ca = 10$. Note the fast relaxation to an axisymmetric droplet at the outset and the subsequent slow relaxation to a spherical shape. Finally, notice the overshoot in q_{33} due to volume preservation of the structural anisotropy tensor

Figure 8 displays the diagonal components of the anisotropy tensor for $\dot{\gamma} = 1$, $Ca = 10$, and four different step shears, $\gamma = (2, 5, 10, 12)$. The arrows in this figure mark the time where the curves for the various components cannot be further distinguished anymore from each other. They give a rough estimate of the time that the droplets need to recover their spherical shape. The shift of the arrows towards increasing times for higher step shears corresponds to a slower effective relaxation of the anisotropy tensor. This increase is also a basic feature of the ALS Model.

The relaxation of the shear stress and the first normal stress difference of the constrained-volume model is presented in Fig. 9 for $\dot{\gamma} = 1$, $Ca = 10$, and the same four step shears of Fig. 8. The points where the droplets have

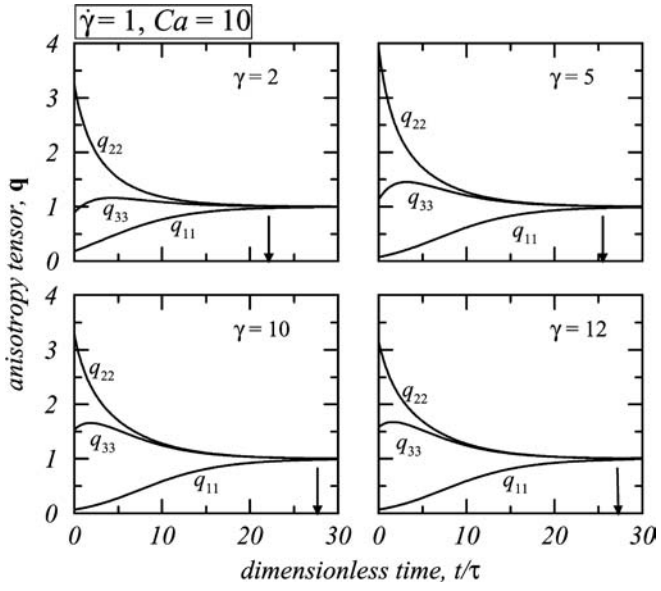

Fig. 8 The diagonal components of the anisotropy tensor as functions of time after various step strains for $\dot{\gamma} = 1$ and $Ca = 10$. The *arrows on the abscissa* indicate the approximate time at which a spherical droplet shape is attained

reached a spherical shape are marked with an arrow in this figure. Note that experimental data on PBd/PDMS blends show a fast decay observed at the beginning of relaxation and a slower decay at later times (Almusallam et al. 2000). The fast decay observed at the beginning of relaxation is believed to be due to relaxation of the deformed ellipsoidal droplets to an axisymmetric shape; however, such a transition from fast to slow relaxation at this point cannot be observed in Fig. 9. This problem can presumably be corrected with an appropriate specification of a non-unit value of the parameter n.

Figure 10 shows the relaxation of the second normal stress difference for the same parameters and the same step shears as those in Figs. 8 and 9. For all cases, there is the characteristic relaxation time to equilibrium, and this appears to be only a function of the fast droplet relaxation mode: after the axisymmetric shape of the droplet has been reestablished, the second normal stress difference vanishes because the appropriate components of **q** have equivalent values.

The thermodynamically consistent model gives a satisfactory description of blend morphology in start up of shear flow as well as in step strain relaxation experiments of polymer blends. The description of the viscometric properties of polymer blends is less satisfactory than the description of the morphological properties. However, keep in mind that we have only investigated the basic physics of the model by adopting a very simple thermodynamic potential and normalizing most parameters out of the model. To achieve better agreement with experimental data, more reasonable parameter values should be adopted.

Conclusion

In this paper we introduced a volume-preserving model for polymer blends that maintains the crucial characteristics of the blend model of Almusallam et al. (2000), while shoring up some of its deficiencies. Specifically, the ALS Model was not completely general for an arbitrary orientation/shape tensor, and the convective contribution to the evolution equation for this tensor was not

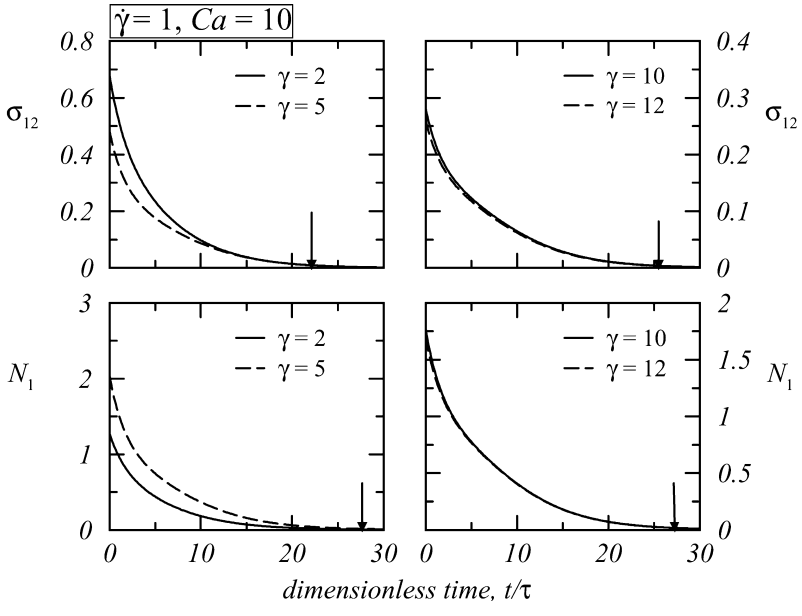

Fig. 9 The elastic shear stress and the first normal stress difference as functions of time after various step strains for $\dot{\gamma} = 1$ and $Ca = 10$. The *arrows* mark the approximate time where the droplets have recovered their spherical shape; they correspond to the times marked in Fig. 8

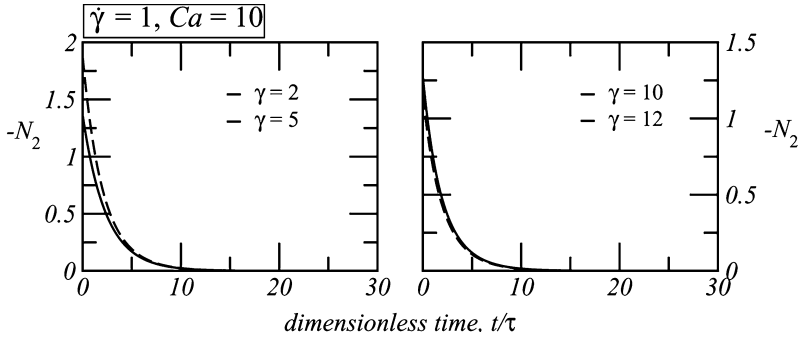

Fig. 10 The second normal stress difference as a function of time after various step strains for $\dot{\gamma} = 1$ and $Ca = 10$

guaranteed to be volume preserving. Furthermore, a different extra stress tensor was calculated that was guaranteed to be compatible with the evolution equation for the orientation tensor. Sample calculations revealed model predictions that always satisfied the constraint of volume conservation, yet were sufficiently wieldable to provide reasonable predictions of real material behavior. At low capillary numbers, the new model attains steady-state much more rapidly than the ALS Model.

References

Ait-Kadi A, Ramazani A, Grmela M, Zhou C (1999) Volume preserving rheological models for polymer melts and solutions using the GENERIC formalism. J Rheol 43:51–72

Almusallam AS, Larson RG, Solomon MJ (2000) A constitutive model for the prediction of ellipsoidal droplet shapes and stresses in immiscible blends. J Rheol 44:1055–1083

Batchelor GK (1970) The stress system in a suspension of force-free particles. J Fluid Mech 41:545–570

Beris AN, Edwards BJ (1990a) Poisson bracket formulation of incompressible flow equations in continuum mechanics. J Rheol 34:55–78

Beris AN, Edwards BJ (1990b) Poisson bracket formulation of viscoelastic flow equations of differential type: a unified approach. J Rheol 34:503–538

Beris AN, Edwards BJ (1994) Thermodynamics of flowing systems. Oxford University Press, New York

Bousmina M, Aouina M, Bushra C, Guénette R, Bretas RES (2001) Rheology of polymer blends: non-linear model for viscoelastic emulsions undergoing high deformation flows. Rheol Acta 40:538–551

Choi SJ, Schowalter WR (1975) Rheological properties of nondilute suspensions of deformable particles. Phys Fluids 18:420–427

Doi M, Ohta T (1991) Dynamics and rheology of complex interfaces. J Chem Phys 95:1242–1248

Dressler M, Edwards BJ, Öttinger HC (1999) Macroscopic thermodynamics of flowing polymeric fluids. Rheol Acta 38:117–136

Edwards BJ, Beris AN (1991a) A unified view of transport phenomena based on the generalized bracket formulation. Ind Eng Chem Res 30:873–881

Edwards BJ, Beris AN (1991b) Noncanonical Poisson bracket for nonlinear elasticity with extensions to viscoelasticity. J Phys A Math Gen 24:2461–2480

Edwards BJ, Beris AN, Grmela M (1991) The dynamical behavior of liquid crystals: a continuum description through generalized brackets. Mol Cryst Liq Cryst 201:51–86

Edwards BJ, Dressler M, Grmela M, Ait-Kadi A (2002) Rheological models with microstructural constraints. Rheo Acta (in press)

Grmela M (1988) Hamiltonian dynamics of incompressible elastic fluids. Phys Lett A 130:81–86

Grmela M (1989) Hamiltonian mechanics of complex fluids. J Phys A Math Gen 22:4375–4394

Grmela M, Ait-Kadi A (1994) Comments on the Doi-Ohta theory of blends. J Non-Newtonian Fluid Mech 55:191–195

Grmela M, Ait-Kadi A (1998) Rheology of inhomogeneous immiscible blends. J Non-Newtonian Fluid Mech 77:191–199

Grmela M, Carreau PJ (1987) Conformation tensor rheological models. J Non-Newtonian Fluid Mech 23:271–294

Grmela M, Öttinger HC (1997) Dynamics and thermodynamics of complex fluids. I. Development of a general formalism. Phys Rev E 56:6620–6632

Grmela M, Ait-Kadi A, Utracki LA (1998) Blends of two immiscible and rheologically different fluids. J Non-Newtonian Fluid Mech 77:253–259

Grmela M, Bousmina M, Palierne JF (2001) On the rheology of immiscible Blends. Rheol Acta 40:560–569

Jansseune T, Vinckier I, Moldenaers P, Mewis J (2001) Transient stresses in immiscible model polymer blends during start-up flows. J Non-Newtonian Fluid Mech 99:167–181

Lacroix C, Grmela M, Carreau PJ (1998) Relationships between rheology and morphology for immiscible molten blends of polypropylene and ethylene copolymers under shear flow. J Rheol 42:41–62

Lee HM, Park OO (1994) Rheology and dynamics of immiscible polymer blends. J Rheol 38:1405–1425

Leonov AI (1976) Nonequilibrium thermodynamics and rheology of viscoelastic polymer media. Rheol Acta 15:85–98

Maffetone PL, Minale M (1998) Equations of change for ellipsoid drops in viscous flow. J Non-Newtonian Fluid Mech 78:227–241. Erratum (1999) 84:105–106

Onuki A (1987) Viscosity enhancement by domains in phase-separating fluids near the critical point: proposal of critical rheology. Phys Rev A 35:5149–5155

Öttinger HC, Grmela M (1997) Dynamics and thermodynamics of complex fluids. II. Illustrations of a general formalism. Phys Rev E 56:6633–6655

Wagner NJ, Öttinger HC, Edwards BJ (1999) Generalized Doi-Ohta model for multiphase flow developed via GENERIC. AIChE J 45:1169–1181